Chromophores and chemical compositions of brown carbon aerosol before and after photooxidation of combustion emissions

Feng Jiang[1,2,5], Jun Zhang[3], David M. Bell[3], Kun Li[3,a], Nadine Borduas-Dedekind[4], Andre S. H. Prevot[3], Hongbiao Cui[1], Harald Saathoff[2*], and Thomas Leisner[2]*

[1]School of Earth and Environment, Anhui University of Science and Technology, Huainan 232001, China

[2]Institute of Meteorology and Climate Research, Karlsruhe Institute of Technology, 76344 Eggenstein–Leopoldshafen, Germany

[3]Laboratory of Atmospheric Chemistry, Paul Scherrer Institute, Villigen5232, Switzerland

[4]Department of Chemistry, University of British Columbia, Vancouver, BC V6T 1Z1, Canada

[5]O'Neill School of Public and Environmental Affairs, Indiana University Bloomington, Indiana 47405, United States

[a]now at: Environmental Research Institute, Shandong University, Qingdao, 266237, Chin

Correspondence to: Feng Jiang (jiangfeng@aust.edu.cn) and Harald Saathoff (harald.saathoff@kit.edu)

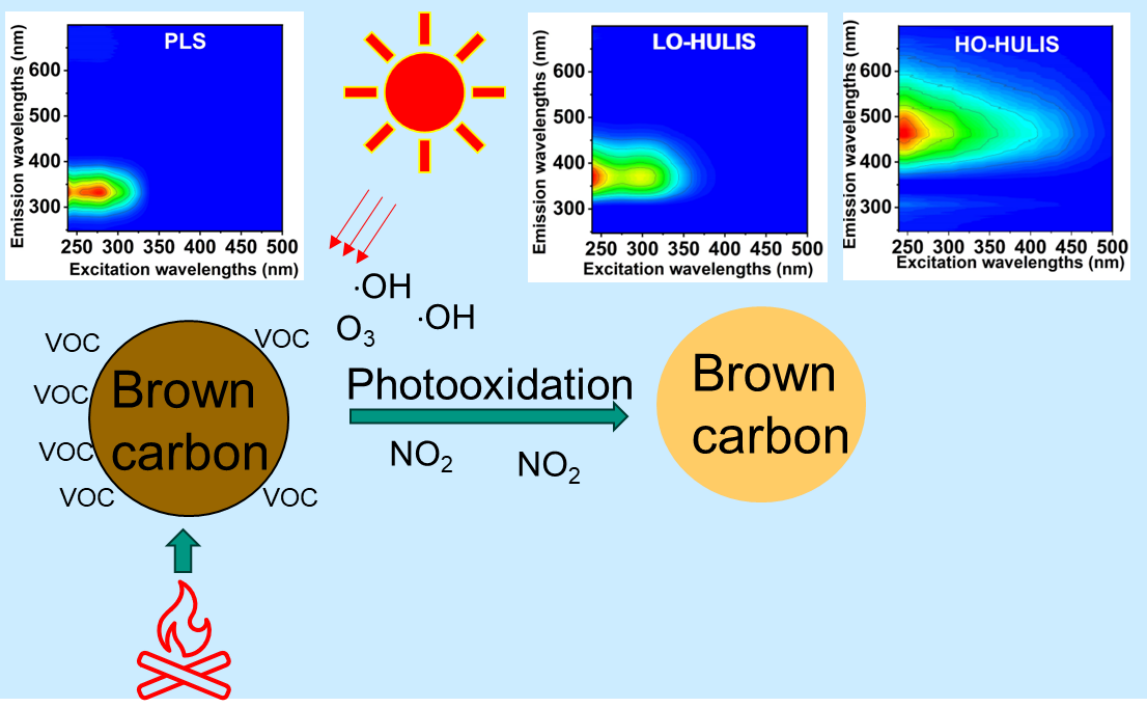

Graphical Abstract

Abstract Brown carbon (BrC) aerosols affect earth's climate and originate mainly from biomass burning. However, chromophores and chemical composition of BrC remain difficult predict, especially considering BrC from different sources and aging e.g. by photooxidation. To address this gap, we studied emissions of burning beech wood, straw, plastics, and cow dung in an oxidative flow reactor allowing to conduct photooxidation aging of fresh emissions by using mass spectrometry and excitation emission spectroscopy with a parallel factor analysis. After photooxidation, volatile organic compounds and heavier molecules were oxidized and formed more oxidized products. Phenolic-like substances (PLS) and less oxygenated humic-like substances (LO-HULIS) dominated the fluorescence of primary organic aerosol with 88 ± 7%. After photooxidation, the PLS chromophore significantly decreased from 45 ± 8% to 10 ± 6% and humic-like substance increased from 55 ± 8% to 90 ± 6%, especially highly-oxygenated humic-like substance (HO-HULIS). The HULIS chromophores were unsaturated and contained high fractions with 5% -10% of nitrogen containing molecules. In contrast, the PLS chromophores had low oxidation states and contained lower fraction (2%) of nitrogen containing molecules. After photooxidation, oxidation of PLS chromophores and volatile organic compounds in presence of NOx were converted into HULIS with the higher fraction of nitrogen containing and unsaturation chromophores. This study extends the current understanding of formation and photochemcial aging of brown carbon chromophorese e.g. PLS, HO-HULIS, and LO-HULIS from open fires including their molecular composition. This will facilitate modelling of brown carbon aerosol e.g. in trasport models.

1. Introduction

Organic aerosols have a profound impact on air quality, human health, and climate. Typically, organic aerosol (OA) is considered to be non-light-absorbing, hence only contributing to scattering of solar radiation that leads to atmospheric cooling (Shrivastava et al., 2017). However, some OA compounds, known as Brown Carbon (BrC), can absorb solar radiation in the near-ultraviolet and visible spectral range contributing to atmospheric warming (Moise et al., 2015; Laskin et al., 2015). Global distributions of aerosol concentrations were simulated with a chemical transport model with a horizontal resolution of 2° × 2.5° and 26 vertical layers from the surface to the top of the atmosphere (Feng et al., 2013). This global simulation showed that the absorption of BrC at ultraviolet-visible wavelengths can contribute 7 - 19% of total atmospheric aerosol absorption (Feng et al., 2013). The global measurement showed that the BrC accounted for 7% - 48% of direct radiative forcing by comparing all absorbing carbonaceous aerosol (Zeng et al., 2020).

The sources of BrC primarily consisted of secondary formation and primary emissions. The secondary formation of BrC was mainly from oxidation of biogenic and anthropogenic volatile organic compounds, especially in the presence of NOx (Jiang et al., 2024; Xie et al., 2017; Yang et al., 2022). The global total primary BrC emissions from natural and anthropogenic sources in 2010 were estimated to 7.26 Tg (Xiong et al., 2022). On a global scale, biomass burning is considered as one of the most important sources for BrC (Laskin et al., 2015; Saleh, 2020). Field-based measurements have shown that a majority of BrC aerosol mass was associated with biomass burning dominating BrC absorption in different areas, e.g, more than 90% in rural southeastern United States (Washenfelder et al., 2015), ~ 60% in Arctic region (Yue et al., 2022), 29%–35% in Himalayas and Tibetan Plateau (Zhu et al., 2024), 50−80% in Israel (Lin et al., 2017), ~60% in central Europe (Moschos et al., 2018). In addition, burning experiments showed that the nitro-aromatics, polycyclic aromatic hydrocarbon derivatives, and polyphenols were important chromophores (molecules responsible for absorbing light and reflecting specific electromagnetic radiation which leading to a color) for brown carbon from wood burning emissions (Lin et al., 2016; Huang et al., 2021). In India, more than half of households use inefficient stoves for cooking, burning solid fuels such as cow dung, firewood, crop residues, and charcoal (Census of India, 2011). This contributes to poor household air quality, chronic and acute respiratory diseases, and even premature

death (Smith et al., 2014). The burning of plastic has been estimated to contribute 13.4% of $PM_{2.5}$ in India, and 6.8% in China (Haque et al., 2019). Previous studies have shown that the BrC chromophores and compositions were different from different biofuels and burning conditions (Huang et al., 2022; Song et al., 2022). Therefore, it is essential to investigate the chromophores and compositions of aerosol particles emitted from burning different fuels.

BrC aging refers to the chemical and photochemical transformation of light-absorbing organic aerosols, a process that is critical because it governs their optical properties, reactivity, and overall atmospheric fates (Laskin et al., 2025). Many studies have investigated the aging process of BrC from the burning combustion emissions. For example, Li et al. (2020)) found that OH radical oxidation and direct photolysis diminished light absorption of wood tar aerosol, since they can decompose the absorption species like nitro-aromatic compounds. The photolysis can fragment chromophore into smaller and less absorbing molecules (Fleming et al., 2020). Sumlin et al. (2017)) found that photooxidation decreased the BrC absorption with 46%, since the fragmentation reactions reduce the size of conjugated molecular system of BrC. Primary BrC from biomass burning with O_3 aging led to decompose protein-like chromophores and form humic-like chromophores (Fan et al., 2020). Sumlin et al. (2017) found that OH radical oxidation can initially enhance brown carbon absorption, followed by bleaching upon further oxidation. Even though the photooxidation and photolysis decreased the light absorption of BrC and decomposed chromophores, it is still uncertain about which chromophores degrade and ultimately the process responsible for the observed changes.

Excitation emission matrix (EEM) fluorescence spectroscopy has been widely used to investigate the chromophore and light absorption of BrC in atmosphere. Combining mass spectrometer and EEM spectroscopy, the chromophore of BrC can be classified into highly oxygenated humic like substances (HO-HULIS), less-oxygenated humic like substances (LO-HULIS), protein compounds (Chen et al., 2016; Chen et al., 2020), and phenol like chromophore (PLS) (Jiang et al., 2022; Tang et al., 2024). In the field measurement, a LO-HULIS chromophore dominated the fluorescence intensity of BrC in winter and, in contrast, HO-HULIS chromophore in summer (Jiang et al., 2022; Deng et al., 2022). The PLS chromophore accounted for 37-51% of total fluorescence of primary BrC from wood burning emission (Fan et al., 2020). Therefore, fluorescence studies are useful to identify the chromophore type of BrC.

However, chemical compositions of BrC chromophores are still not well known, especially for particles from biomass burning.

The filter inlet for gases and aerosols coupled to a high-resolution time-of-flight chemical ionization mass spectrometer (FIGAERO–HR-ToF-CIMS) can provide new insights into the molecular compositions of organic aerosol (Lopez-Hilfiker et al., 2014). For example, Kong et al. (2021)) found that the chemical compositions of primary particles were composed of lignin pyrolysis products, cellulose and hemicellulose pyrolysis products, and nitrogen-containing compounds in a residential wood burning boiler experiment. Several studies have also used CIMS to identify nitro aromatic compounds, typical brown carbon (Cai et al., 2022; Mohr et al., 2013; Salvador et al., 2021). In addition, Jiang et al. (2022)) used the CIMS to identify 316 potential BrC molecules and 5 nitro aromatic compounds in field measurements. Therefore, the CIMS is a useful instrument to detect the chemical composition of organic aerosol and BrC. Combining FIGAERO-CIMS and excitation emission spectroscopy, it is helpful to link chromophores and the chemical composition of primary BrC from burning combustion emission.

In this study, we investigated the influence of fuel type and photochemical aging on the optical and chemical properties of primary and secondary BrC. Burning different fuels generated primary particles and gases which were subsequently oxidized forming secondary organic aerosol mass. Burning combustion emission experiments generated primary particles. The burning fuels are wood beech, straw, cow dung, and plastic. Followingly, the primary particles, volatile organic compounds, and trace gases were flowed into simulation chamber and underwent photooxidation aging process. The chromophore and chemical composition of BrC will be detected by excitation emission spectroscopy and FIGAERO-CIMS, respectively. This work allows for a better understanding of the changing of chromophore and chemical composition of BrC from primary burning emissions.

2. Experimental methods

2.1. Experimental setup

A total of 4 burning experiments were conducted using 4 different types of burning materials, including beech, straw, cow dung, and plastic, as shown in Table S1 in the supplement. Please note that each burning experiment had no replicate experiment. This could lead to uncertainties in the results since the biomass burning experiments involve inherent variability. The burning materials are described in more

detail by previous publications (Zhang et al., 2023; Wang et al., 2025; Li et al., 2024). Briefly, the straw and beech were sourced from a local forestry company in Würenlingen, Switzerland. The cow dung cakes (made of cow dung and straw) were sourced from Goyla dairy, Delhi, India and polyethylene plastic materials were bought in Delhi, India. We categorized four burning types for this experiment: beech, cow dung, straw, and plastic. We selected these four solid fuels and conducted emissions tests to simulate certain types of burning in the atmosphere. The beech, straw, and cow dung are representative of residential wood burning, which is consistent with the materials used in previous articles (Zhang et al., 2023; Li et al., 2024; Wang et al., 2025). The polyethylene plastic materials are representative of plastic burning in India and China (Haque et al., 2019).

The burning straw and beech in an open stainless-steel cylinder were presented as agricultural waste combustion and forest fires, respectively. The stainless-steel cylinder is 62 cm in diameter and 35 cm in height. This cylinder has been used to investigate wood beech burning emissions in the previous studies (Sardena et al., 2026; Bogler et al., 2025). The burning cow dung and plastic materials on top of stainless-steel cylinder were presented as waste burning in India (Zhang et al., 2023; Wang et al., 2025). In addition, the cow dung and plastic burning on the top of stainless-steel cylinder was more efficiency than in the stainless-steel cylinder. The experimental setup is shown in Fig. S1 in the Supplement. The fuels were ignited with kindling, and the emissions were pulled into a hood. After the kindling burned away (~3 to 10 minutes after ignition), the emissions were introduced into a holding tank through stainless steel sampling lines and passing through an ejection dilutor (DI-1000, Dekati Ltd.) with a dilution ratio of ~10. The holding tank is a stainless-steel container (1 m^3) used to store emissions. The aim of holding tank is to average the emissions at different combustion efficiency in order to fully characterize the emission in ambient (Zhang et al., 2023). The holding tank was flushed overnight with clean air before each experiment, ensuring the background particle concentrations were less than 10 particles cm^{-3}. To avoid cross-contamination from residual SVOCs in the holding tank, it was flushed overnight with clean air before each experiment, ensuring the background particle concentrations were less than 10 particles cm^{-3}. This way residual SVOCs did not significantly affect subsequent measurements (Li et al., 2024). The emissions were injected into the holding tank for 10 to 30 minutes, depending on the emission source (Zhang et al., 2023). When the particle mass concentration was between 1 to 5 mg m^{-3}, we stopped injecting particles into the holding tank. The particles in the holding tank were collected by quartz filters

and Teflon filters and samples can be considered as primary organic aerosol. Blank quartz and Teflon filters were collected during the campaign and analyzed in the same way as the other samples. Please note that quartz filters and Teflon filters have different adsorption behaviour of gases which could lead to different filter loading and hence differences between EEM and mass spectrical analysis. However, due to sufficient particle mass loading on the filters, the potential contribution of this effect can be considered as minor

The holding tank was connected to an oxidative flow reactor (OFR) to generate secondary organic aerosol from the volatile organic compounds and NOx present in the holding tank. Please note that the NOx was generated during the burning. There were no instruments to measure the NOx concentration. However, according to previous studies, the concentrations of NOx were around a few hundred ppm (Winter et al., 1999; Courtemanche and Levendis, 1998). Furthermore, the volatile organic compounds were generated from the combustion (Li et al., 2024). After the filter collection of the primary organic aerosol (POA), an aged OA filter was collected including both the POA and secondary organic aerosol (SOA) generated in the OFR. The OFR was maintained at 293 K and 50% relative humidity, and a constant O_3 concentration of 4 ppm was present. The OFR has 254 nm lights, which photolyzes O_3 to produce OH radicals (Li et al., 2024). The OH exposure was set to 5.4×10^{11} molecules cm^{-3} s during the experiment (Li et al., 2024). The holding chamber provided a constant source of VOCs and POA to generate SOA (Li et al., 2024; Wang et al., 2025). The output of the OFR was directed to either a quartz or Teflon filter. Similar to previous studies (Li et al., 2024), ~50 μg m^{-3} of POA entered the OFR and ~50-100 μg m^{-3} of SOA was formed in the OFR. Unfortunately, there was not a concurrent measurement of aerosol mass concentration during filter collection since the entire output of the OFR was directed to the filter samples. Therefore, it is not possible to discuss the results below in quantitative terms. Since the samples contain primary emissions and secondary aerosol, we named these filters as the aged organic aerosol e.g. Figure 1. It is helpful to classify our samples. Before starting the experiments, the background filters were collected. The filter samples are shown in Table S1. For this paper, we will mainly discuss the results from excitation emission spectroscopy and FIGAERO-CIMS measurements.

2.2. FIGAERO-CIMS analysis of filter samples

Teflon filters collected at different phases of experiments were analyzed with a filter inlet for gases and aerosols coupled to a high-resolution time-of-flight chemical ionization mass spectrometer (FIGAERO-HR-ToF-CIMS, Aerodyne Research Inc. hereafter CIMS) employing iodide (I^-) for chemical ionization (Jiang et al., 2022; Lopez-Hilfiker et al., 2014) which provide information of individual organic compounds. In brief, particles on the Teflon filter were desorbed by a flow of ultra-high-purity nitrogen (99.9999 %) heated from room temperature to 200 ºC over the course of 35 min (Lopez-Hilfiker et al., 2014; Huang et al., 2019). The resulting mass spectral signal evolutions as a function of desorption temperature are termed thermograms (Lopez-Hilfiker et al., 2014). Integration of thermograms of individual compounds yielded their signal in counts per second, which were converted to mass concentrations assuming an average maximum sensitivity of 22 counts s^{-1} ppt^{-1} (cps ppt^{-1}, ppt: parts per trillion) (Lopez-Hilfiker et al., 2014). Please note that the sensitivity of CIMS for different organic compounds can vary by a few orders of magnitude.

During the measurements, the mass resolution of FIGAERO-CIMS was relatively stable with about 4000 m/Δ. The interference from isomers with different vapor pressures or thermal fragmentation of larger oligomeric molecules can lead to more complex, multimodal and broader thermograms (Lopez-Hilfiker et al., 2014). The signal integration can include the different isomers or thermal fragmentation of larger oligomers. Therefore, the isomers or thermal decomposition can lead to increase errors of estimating the organic mass concentrations (Jiang et al., 2024). In this study, organic molecules of Teflon filters were identified by FIGAERO-CIMS. Please note that the iodide CIMS has sensitivities varying over several orders magnitude for different compounds, for example, different oxidation states (Lopez-Hilfiker et al., 2016). Keeping this in mind, it can still be meaningful to do a relative comparison of the large number of highly oxidized compounds assuming the same sensitivity. The raw data were analysed using the toolkit Tofware (v3.1.2, Tofwerk, Thun, Switzerland, and Aerodyne, Billerica) with Igor Pro software (v7.08, Wavemetrics, Portland, OR). Particle-phase backgrounds were assessed by putting an additional clean Teflon filter upstream of the particle phase sampling port during the deposition (Huang et al., 2019; Lee et al., 2018). In this study, we observed typically about 2800 mass peaks from particles corresponding to different oxygenated organic compounds using FIGAERO-CIMS.

2.3. Excitation emission spectra of methanol-soluble compounds

Methanol-soluble organic carbon (MSOC) was extracted from the quartz filters with 5 mL methanol (for analysis purity, Merck) via ultrasonication of filter punches for 30 min. The methanol extraction had high extraction efficiency for organic compounds on the filters. Obtained extracts were filtered through a 0.45 μm polytetrafluoroethylene membrane into a glass bottle to remove the insoluble material. Please note that the MSOC contains methanol-soluble but also water-soluble compounds since also water-soluble compounds are partially soluble in methanol. We did this direct methanol extraction in order to dissolve a maximum number of compounds facilitating a good comparison with the mass spectrometric analysis in which there is no differentiation between different solubilities. However, this has to be kept in mind when comparing our results with studies that separated the water and methanol soluble fractions. Absorption and excitation– emission spectra of these extracts were measured by an Aqualog fluorometer (HORIBA Scientific, USA). Please note that since the organic mass loadings were not clear, we did not calculate the mass absorption coefficients. The Aqualog measurements were described by previous studies (Jiang et al., 2022). In the brief, we used an excitation wavelength range from 239–500 nm and an emission wavelength range from 247–700 nm. The wavelength increments of the scans for excitation and emissions were 3nm and 2.33 nm, respectively. The resulting excitation–emission spectra were analyzed with the PARAFAC model to identify potential chromophoric components in MSOC.

The details of the data analysis procedure are given by Pucher et al. (2019) and Murphy et al. (2013). We used the StaRdom package for RStudio version 2026.04.0 of PARAFAC model (Pucher et al., 2019), which was downloaded from https://cran.r-project.org/web//packages/staRdom/vignettes/PARAFAC_analysis_of_EEM.html (last access: 19 February 2026). In brief, light absorption measurements were used to correct the excitation-emission matrices (EEM) for inner-filter effects. The highest absorbance was not greater than 2 (mostly below 0.5 at 237 nm), which is appropriate for inner-filter corrections of the EEMs. Afterwards, all EEMs were normalized to the Raman peak area of water so that their unit is in Raman units (RU) whose excitation wavelength was 350 nm. Additionally, an interpolation method was used to remove the signals of the first-order Rayleigh and Raman scattering as well as the second-order Rayleigh scattering in the EEMs. Using all 8 EEMs obtained for combustion emission particles in the PARAFAC analysis, three different components were adopted by comparisons of the residual errors and by visual inspection for the three-

to seven component PARAFAC model (Figure 2). They successfully passed the split-half validation with the split style of S4C6T3 for the 8 samples (Fig. S2). The corresponding model parameters and detailed information of the Split-half validation are shown in Table S2 and following contents.

2.4. Statistical analysis

The PARAFAC component intensities were normalized to the sum of components fluorescence intensities for given samples. The mass concentration of each molecule was normalized by the total mass concentration of 2871 organic molecules detected by FIGAERO-CIMS. The Spearman correlations were derived between each molecule and PARAFAC data across 8 samples (straw fresh OA, straw aged OA, plastic fresh OA, plastic aged OA, beech fresh OA, beech aged OA, cow dung fresh OA, and cow dung aged OA). The molecules correlated to PARAFAC component intensities with Spearman ≥ 0.643 (one tailed test, see the detailed information in the supplement section 2) were assigned to each PARAFAC component (Table S5, S6, and S7) (Tang et al., 2024; Stubbins et al., 2014). The molecular formulas were categorized into four groups based on their Modified Aromaticity Index (AI_{mod}) and H/C ratio, e.g, condensed aromatic compounds ($AI_{mod} \geq 0.67$); aromatic compounds ($0.5 < AI_{mod} < 0.67$); highly unsaturated and phenolic compounds ($H/C < 1.5$, $AI_{mod} \leq 0.5$); and aliphatic compounds ($1.5 \leq H/C \leq 2.5$).

3. RESULTS AND DISCUSSION

3.1 Chemical composition of aerosol particles from combustion emissions

3.1.1 Chemical composition of fresh OAs from combustion emissions

Fresh OA from combustion of beech wood, straw, plastics, and dried cow dung formed in smog chamber oxidation experiments were collected on Teflon filters and analysed by FIGAERO-CIMS for the oxygenated organic compounds. Average mass spectra for particles formed for these four cases are presented in Figure 1.

The highest signal intensity was observed for levoglucosan ($C_6H_{10}O_5$) accounting for 10%–35% of the total signal intensities from FIGAERO-CIMS (Table S3). This is consistent with previous studies in which levoglucosan was considered as a typical tracer for biomass burning (Bhattarai et al., 2019). In addition, levogluscon in POA from wood, straw, and cow dung contributed ~7% to ~30% of the total intensity measured by the extractive electrospray ionization time-of-flight mass spectrometer (EESI-ToF-MS) (Zhang et al., 2023). In natural burning, the mass fraction of sugar derivatives ($C_5H_8O_4$, $C_8H_{12}O_6$, $C_6H_{12}O_5$) was higher (6.7 ± 3.5%) than that in plastic burning (4.9%). It indicates that natural burning produces more sugar derivatives than plastic burning on average, but these compounds are not a definitive tracer for distinguishing them. $C_8H_{12}O_6$ and $C_5H_8O_4$ had also significant contributions of 1%-6% to the total signals of particles from combustion of beech wood, straw, cow dung, and plastic fresh OA. Zhang et al. (2023) found that $C_8H_{12}O_6$ was a dominant compounds with fractions of ~2% to ~9 % in POA from wood, straw, and cow dung. Kong et al. (2021) also found that $C_8H_{12}O_6$ and $C_5H_8O_4$ of POA from combustion emission of birch, spruce and aspen had important signals in CIMS measurement. Interestingly, comparing the combustion products from the four fuels, compounds at higher mass ranges (m/z including I-:450 – 650) were formed mainly from straw, cow dung, and plastic. For fresh OA from straw-burning emission, $C_{27}H_{54}O_2$, $C_{28}H_{56}O_2$, $C_{29}H_{58}NO_2$, and $C_{32}H_{64}O_2$ showed relatively high fractions with ~0.6 – ~1.4%. For fresh OA from cow-dung burning emissions, $C_{29}H_{58}NO_2$, $C_{32}H_{64}O_2$, and $C_{32}H_{66}N_3O$ showed high contributions with 1%–2%. For fresh OA from plastic burning emission, $C_{16}H_{32}O_2$, $C_{18}H_{32,34,36}O_2$, and $C_{24}H_{44,48}O_2$ showed high contributions with ~0.6 – ~1.5%. Those compounds with large molecular mass are likely to be common saturated and unsaturated fatty acids

(Simoneit, 2002). Nitro-aromatic compounds ($C_7H_7NO_4$, $C_6H_5NO_4$, and $C_8H_9NO_4$) had lower fractions (0.3%–0.9%) on the burning products from primary emissions. Zhang et al. (2022)) found that the nitro aromatic compounds emission factors varied by more than 2 orders of magnitude and the concentrations ranged from 6.47 ng m^{-3} in the burning of briquette coal in the traditional stove to 2560 ng m^{-3} in the sesame straw burning. Therefore, the emission of nitro aromatic compounds emissions varied in large range depending on the type of burning occurring and the incorporation of nitrogen in the burning materials.

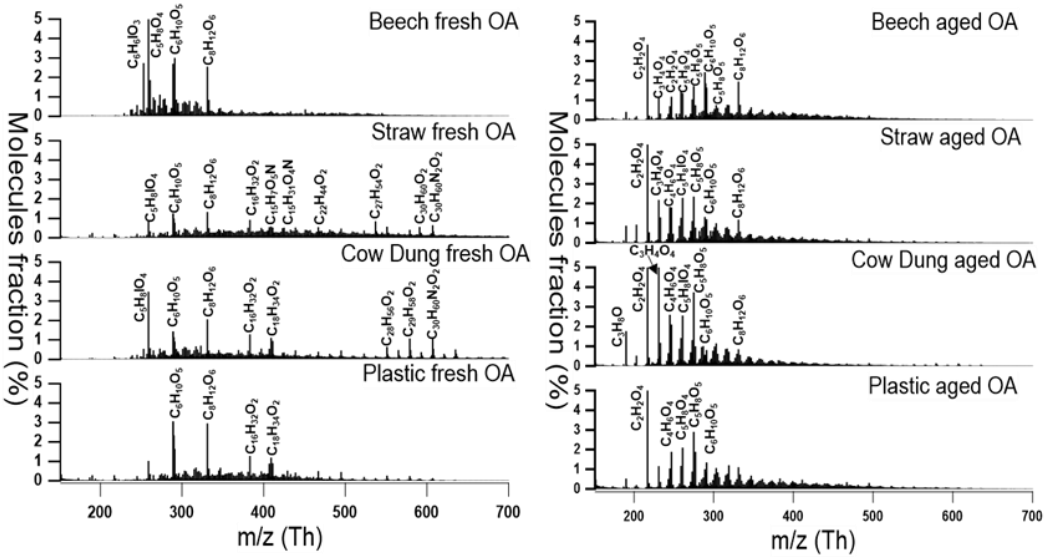

Figure 1. Mass spectra with iodide of particles from fresh OA and aged OA combustion emissions from FIGAERO-CIMS measurements. Particles from combustion/oxidation of beech wood; straw; plastics; cow dung. Please note that the signal intensity of levoglucosan ($C_6H_{10}O_5$) was multiplied by 0.1. Please note that the samples contain both primary emissions and secondary aerosol after photooxidation, we named these samples as aged organic aerosol.

3.1.2 Chemcial composition of aged OA from photooxidation

Figure 1 shows the major aged OA molecules formed by subsequent oxidation of the primary emissions from the burning fuels. The mass fraction of heavier molecules was reduced and lighter more oxidized compounds like small organic acids increased (Table S4). After photooxidation, $C_6H_{10}O_5$ in plastic fuels showed a 66% decrease, which was larger than that in straw, Cow dung and beech fuels. The mass fraction of lighter molecules increased because of the formation of photochemical oxidation of volatile organic compounds (VOCs) generating SOA (Li et al., 2024). Li et al. (2024) also found that oxidation of volatile organic compounds from biomass burning was a major source of secondary organic aerosols

(SOAs). The aged OA by in large has smaller moleculer weights than those present in the fresh OA. As shown in Figure S3, after photooxidation of the fresh OA, all O/C ratios increased between 0.1–0.4 with largest increases for straw and cow dung. The mass fraction of smaller organic acids (C2-C5) of aged OA in straw and cow dung were 24% and 34% higher than 12% and 18% in beech and plastic. The higher enhancement of O/C ratio of aged OA in straw and cow dung is caused by the higher contributions of smaller organic acids. Kodros et al. (2022)) also found that the oxidation of biomass burning aerosol leads to an increase in O/C ratios ranging from 0.09–0.23 (enhancement of 1.2–1.58) after the injection of NO_2 and O_3 for 3 hours. Yazdani et al. (2023) found that the biomass burning secondary OA became more oxidized with continued aging and the productions were dominated by acids. Kodros et al. (2020)) found that the composition of the biomass burning OA evolves dramatically under oxidation and the O/C increased from 1.2 to 1.5.

3.2 Chromophore identification and abundance in fresh OA

Filter samples collected for the eight different cases were dissolved by methanol and measured their absorption and excitation-emission spectra. A PARAFAC model was used to investigate the major chromophores in methanol-soluble organic carbon extracted from the biomass-burning aerosol particles (Chen et al., 2020). With this approach, three different characteristic chromophore components were identified and named C1, C2, and C3, hereafter (Figure 2). The peaks of excitation/emission (Ex/Em) values for C1 were at 239, 300 nm for excitation and at 372 nm for emission. Correlation analysis of PARAFAC components and Aerosol Mass Spectrometer data resulted that a similar water-soluble chromophore component can be considered as less-oxygenated humic-like substances (Chen et al., 2016). The peak of excitation/emission (Ex/Em) values for C2 was at 245 nm for excitation and at 372 nm for emissions. The maximum emission wavelength of C2 ranges above 400 nm. Similar components as C2 were found in water-soluble organic carbon and considered highly oxygenated humic-like substances (Chen et al., 2016; Yan and Kim, 2017). The maximum emission wavelength of C3 was less than 350 nm. It was located at the phenolic-like region which contains phenol and naphthalene compounds (Jiang et al., 2022), since the peaks of shorter excitation wavelength (<250 nm) and shorter emission wavelength (<350 nm) were associated with aromatic proteins like tyrosine (Cory and Mcknight, 2005). Jiang et al. (2022)) found that phenol- and naphthalene-like components had a good correlation ($r = 0.7$) with phenol, which most likely originates from biomass burning and fossil fuel combustion. Compared with the

significant similarity of the characteristic spectra identified using the PARAFAC model with literature data, C1 was considered as a less-oxygenated HULIS (LO-HULIS), C2 as a highly oxygenated HULIS (HO-HULIS), C3 as a phenolic-like substance (PLS).

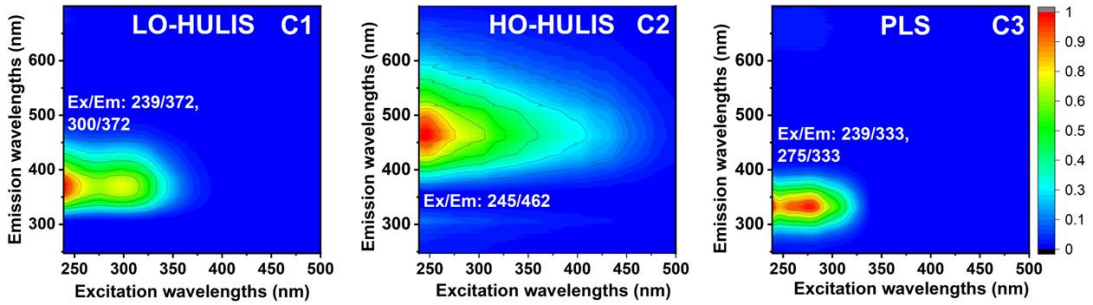

Figure 2. The three chromophores were identified by the PARAFAC model analysis of the excitation–emission spectra from all filter extracts collected from combustion of beech wood, straw, cow dung, and plastic.

Figure 3 shows that there were different relative contributions of chromophore components from burning the four different fuels. The LO-HULIS has a relatively high contribution of (45 ± 10%) in biomass-burning fresh OA. The LO-HULIS was also identified as chromophore in brown carbon from biomass burning (straw, pinewood, and corn straw) with a contribution of 15% – 25% (Fan et al., 2020). Tang et al. (2020)) found that a similar chromophore was enriched in biomass burning aerosol with a fraction of 21 ± 6.9 %. The relative contribution of LO-HULIS was with 56% ± 7% higher for beech wood than for the other three fuels with all nearly 40%. However, compared to LO-HULIS, the HO-HULIS in four different fuels shows only lower contributions to fluorescence with 14% ± 8%. This is in contrast to findings by Jiang et al. (2022)) who found that the HO-HULIS components dominated (96 ± 6) % in summer and had much less but still substantial contributions of (31 ± 8) % in winter, both for urban aerosol. However, this finding somewhat agrees with the HO-HULIS fraction of about 10% of brown carbon POA from pinewood burning (Fan et al., 2020). In contrast to LO-HULIS, the relative contribution of the PLS in four different fuels was higher with 40% ± 12% which has an important contribution to the chromophore. This is consistent with a previous study where a similar component dominated the fluorescence in biomass-burning aerosol with about 35% – 45% (Fan et al., 2020).

3.3 Chromophore variations after photooxidation

Variations of the relative chromophore contributions for the oxidized primary emissions of the four fuels are displayed in Figure 3 as well. After aging with ozone and OH radicals during photooxidation, the

relative contribution of PLS significantly decreased, from 54% to 8% for plastic, from 33% to 5% for straw, from 52% to 9% for beech wood, and from 43% to 20% for cow dung. These findings suggest that the phenolic-like chromophore is easily susceptible to photooxidation. The HO-HULIS exhibits a significant increase with photooxidation from 5% to 46% for plastic, from 23% to 34% for straw, from 12% to 31% for beech wood, and from 8% to 19% for cow dung. This indicates that excitation-emission associated with HO-HULIS increased substantially with the formation of secondary organic aerosol (SOA) and SOA is the dominant contributor to HO-HULIS. In comparison, the LO-HULIS also moderately increased, from 41% to 47% for plastic, from 44% to 61% for straw, from 36% to 60% for beech wood, and from 49% to 61% for cow dung. Taken together, the relative contributions of humic-like fluorophores (LO-HULIS and HO-HULIS) accounted for 77%–91% of the aged combustion BrC (aged OA), which is much higher than the range of 44%–55% observed for the primary samples (fresh OA). Consistently, after photooxidation, smaller m/z organic molecules were formed from SOA formation (Figure 1). The major difference after SOA formation is the shift in the emission spectra from lower wavelengths (333 – 370 nm) to higher wavlengths (462 nm).

Correspondingly, the O/C ratio increased with an enhancement of 0.1–0.4 (Figure S3). Compared with previous studies, the O_3 oxidation of oxyaromatics could produce polyhydroxylated aromatics (Fan et al., 2020). Fan et al. (2020)) also found that a component (protein-like or phenol-like organic matter, PLOM) similar as PLS was predominantly decomposed by ozone aging, while the relative fraction of highly oxygenated humic-like components significantly increased. Though, ozonolysis of biomass burning POA generated from wood combustion is relatively minor on the time scale of oxdative flow reactor, where the O:C ratio increased by ~10% (Bogler et al., 2025).

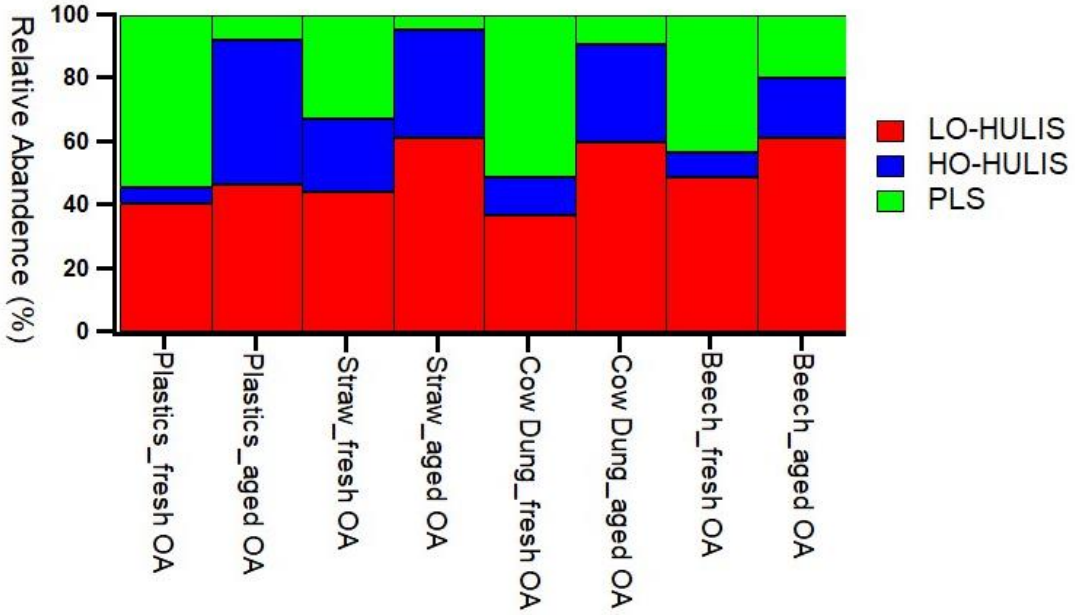

Figure 3. Relative contribution of the three chromophore components identified by PARAFAC model analysis to total fluorescence. Comparison of relative contributions from fresh OA and aged OA from combustion of the four different fuels.

3.4 Molecular signatures of PARAFAC chromophores

The chemical composition of organic aerosol could be assigned to the three different chromophores factors (LO-HULIS, HO-HULIS, and PLS) identified by the PARAFAC analysis based on their individual correlations. The detailed correlation and assignments are shown in supplement section 2 and Table S5, S6, and S7. The properties of molecules related to the three chromophore components are given in Table 1. As shown in Table S5, 49 molecules were associated with LO-HULIS chromophore and accounted for 6.5 ± 4.2% of total organic molecules detected by FIGAERO-CIMS. The number of LO-HULIS assocated molucules was lower than HO-HULIS and PLS. Compared with HO-HULIS and PLS, LO-HULIS molecules showed a relatively low molecular weight (156.6 Da), an low O/C ratio of 0.6, higher unsaturation degrees (DBE and AI_{mod}), higher level of condensed aromatic compounds (23.4%), and higher fractions of highly unsaturated and phenolic compounds (36.0%) (Figure 4a, Table 1). This indicates that LO-HULIS chromophores were highly unsaturated and have high fractions of highly unsaturated and phenolic compounds. Consistently, Jiang et al. (2022)) found that a similar chromophore group as HO-HULIS had a high DBE (5.8 ± 0.04), a high AI_{mod} (0.23 ± 0.02), and a relatively low average O/C ratio of 0.8 ± 0.01 in field meaasurments.

Table 1. The average properties of molecules were associated to three characteristic chromophores. The number of average molecular mass, averages molecular properties, and structural grouping of molecular formulas as determined by FIGAERO-CIMS in 8 samples. These were founded to correlate with each of the 3 fluorescence PARAFAC components identified (LO-HULIS, HO-HULIS, and PLS); and those which did not correlate with any the PARAFAC component (Not included).

Average properties	LO-HULIS	HO-HULIS	PLS
Molecular mass (Da)	156.6	171.9	206.7
O/C ratio	0.6	0.8	0.5
H/C	1.2	1.3	1.5
DBE	4.4	4.1	3.5
AI mod	0.4	0.3	0.1
OSc	0.1	0.3	-0.4
Mass fraction of nitrogen containing molecules (%)	7.5	12.9	4.3
Condensed aromatic compounds (%)	30.0	27.6	6.2
Aromatic compounds (%)	10.4	3.2	5.3
Highly unsaturated and phenolic compounds (%)	36.0	21.3	27.8
Aliphatic compounds (%)	22.8	44.9	60.7

The 143 molecules associated with HO-HULIS chromophore accounted for 5.9 ± 4.4% of total organic molecular signals detected by FIGAERO-CIMS. The number of molucules assocated with HO-HULIS was higher than LO-HULIS and PLS. Compared with LO-HULIS and PLS, HO-HULIS molecules showed a middle level of molecular weight (171.9 Da), higher O/C ratio (0.8), higher OSc (0.3), higher fraction of nitrogen containning molecules, and lower fractions of highly unsaturated and phenolic compounds (21.3%) (Figure 4b, Table 1). Therefore, it indicates that the HO-HULIS chromophore was more oxidized and contained high fraction of nitrogen containing molecules. Compared with previous studies, a samilar chromphore as HO-HULIS shown that the average O/C ratio, molecular weight, DBE, and AI_{mod} were 0.9 ± 0.01, 170 ± 1 Da, 3.6 ± 0.03, and 0.16 ± 0.01, respectively (Jiang et al., 2022). Tang et al. (2024)) found that a similar chomophore as HO-HULIS had more than 60% of nigrogen containing molecules. In addition, the HO-HULIS chromophore was associated with more compounds that possessed higher aromaticity (AI_{mod} > 0.5) and higher oxidation state (OSC > 0) (Tang et al., 2024).

The 108 molecules associated with PLS chromophore accounted for 12.8 ± 7.6% of total organic molecules detected by FIGAERO-CIMS. Compared with LO-HULIS and HO-HULIS, these molecules show a higher molecular mass (206.7 Da), lower O/C ratio (0.6), higher H/C ratio (1.5), lower unsaturation degrees (DBE and AI_{mod}), lower OSc (-0.4), low fraction of nitrogen containing molecules (2%), and higher fraction of aliphatic compounds (Figure 4c, Table 1). In addition, the associated molecules of PLS chromophores had some monomers or dimmers, e.g., $C_{16}H_{14}O_2$, $C_{18}H_{32}O_2$, $C_{18}H_{34}O_2$, $C_{18}H_{35}O_2N_3$, etc. Therefore, it indicates that the PLS chromophore was low oxidation state, contained lower fraction of nitrogen containing molecules and higher fraction of aliphatic compounds. Compared with previous stuides, the PLS chromophore was not exclusively associated with nitrogen-contianing compounds (Tang et al., 2024; Stubbins et al., 2014). Tang et al. (2024)) found that PLS chromophore in a field measurment was consisted of lowconjugation, nitrogen-depleted, and oxygen-depleted species.

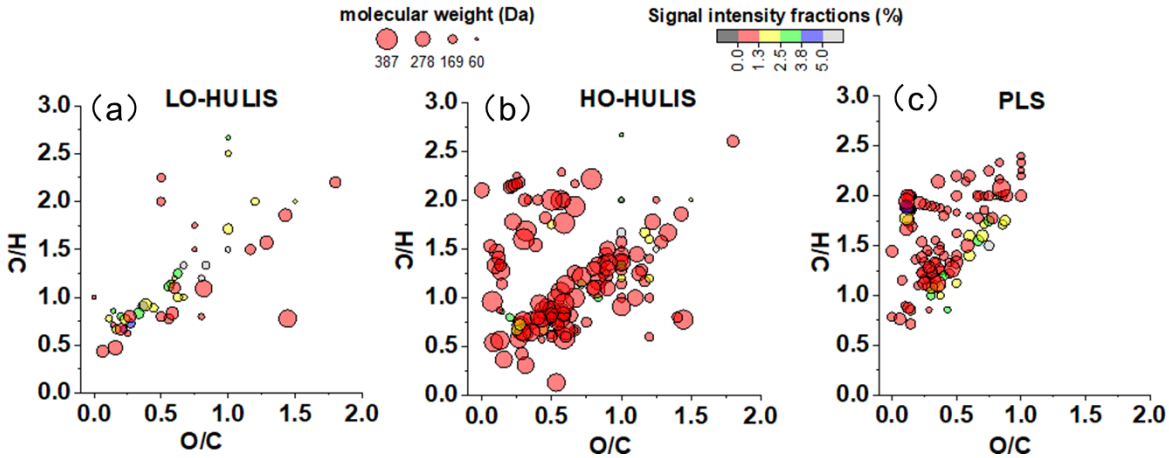

Figure 4. Van Krevelen diagrams of FIGAERO-CIMS identified compounds assigned to PARAFAC components (LO-HULIS, HO-HULIS, and PLS).

3.5 Potential mechanisms of PLS decreasing and HULIS formation during the photooxidation

After photooxidation, the relative contents of the PLS chromophore decreased. The photooxidation of PLS and volatile organic compounds in presence of NOx could lead to form the HO-HULIS and LO-HULIS (Figure 3). Please note that the NOx was generated during the burning. According to previous studies, the concentrations of NOx were around a few hundred ppm (Winter et al., 1999; Courtemanche and Levendis, 1998). The conceptual illustration is shown in Figure 5. The PLS chromophore contained molecules with lower-conjugation, lower nitrogen content, and lower oxygen content. During the photooxidation, the PLS molecules were oxidized by O_3 and OH radicals in presence of NOx. The

chemcial bonds in large molecules ($C_{9.9}H_{14.8}N_{0.05}O_{4.5}$) were broken. In addition, the photooxidation of VOCs in presence of NOx can formed the small molecules with higher fractions of nitrogen-containing molecules and higher oxidation state (Li et al., 2024). Consequencely, they led to form LO-HULIS ($C_{7.2}H_{7.7}N_{0.1}O_{3.8}$) and HO-HULIS ($C_{7.3}H_{8.6}N_{0.2}O_{4.6}$) with higher O/C ratio and lower H/C ratio. Consistently, the O_3 oxidation of oxy-aromatics can cause the cleavage of the aromatic bond (C=C) to generate polyfunctional low-molecular-weight carboxylic acids (C=O) and also formation of polyhydroxylated aromatics (phenol-OH) (Fan et al., 2020). However, evolutions of chromophore were different at ambinent environments compared with primary aerosol at chamber experiments. For example, the photochemical reaction and oxidation reaction drive degradation of less-oxygenated humic-like substances and led to forming highly-oxygenated humic-like substances (Chen et al., 2021a; Chen et al., 2021b). This study has not yet achieved quantitative characterization of each individual process (the degradation of large molecules and oxidation of VOCs) contributing to HULIS chormophore formation. Future studies need to integrate isotopic techniques or mass spectromters to address this limitation and accurately quantify the contribution of each process.

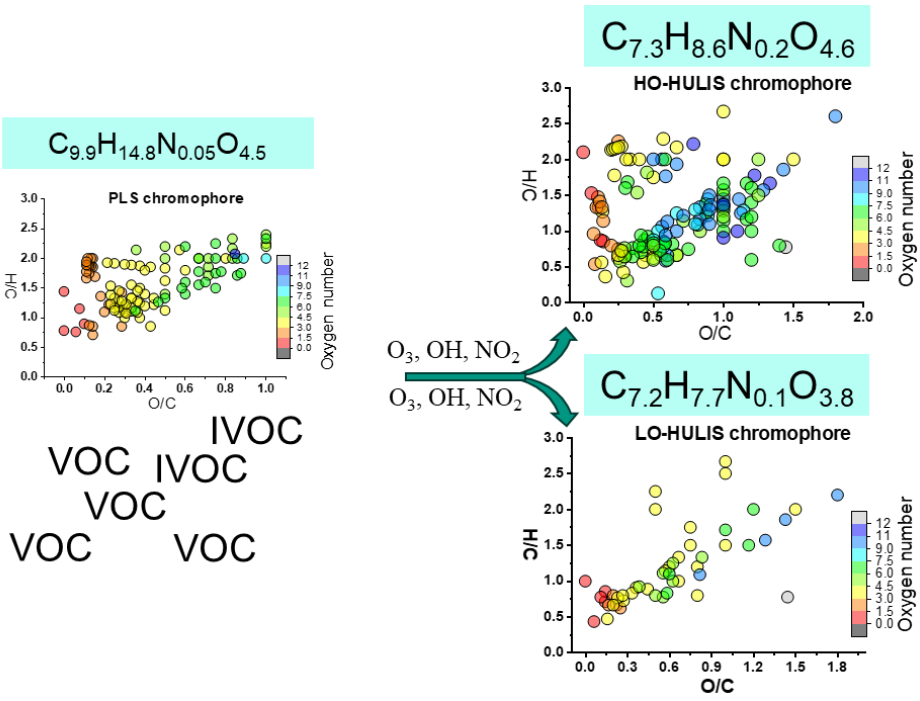

Figure 5. The PLS associated molecules and VOCs were oxidized into HO-HULIS associated molecules and LO-HULIS associated molecules during the photooxidation in the presence of NOx.

4. Conclusions

The chemical composition and the corresponding optical properties of aerosol particles from combustion of straw, beech wood, plastic, and cow dung and their subsequent aging by photooxidation were comprehensively characterized using mass spectrometry (FIGAERO-CIMS) and excitation emission spectroscopy (Aqualog) as well as a series of supplementary instruments. Levoglucosan ($C_6H_{10}O_5$) dominated the oxygenated compounds with the total signal intensities of 10%–35% from FIGAERO-CIMS. After photooxidation, the heavier molecules were less abundant partially due to fragmentation but also due to gas to particle partitioning of lighter molecules formed by oxidation reactions in the gas phase e.g. $C_2H_2O_4$ and $C_3H_4O_4$. In addition, the O/C ratio increased by 0.1 – 0.4. This indicates that aging of the primary combustion emissions in presence of photooxidation lead to higher O/C ratios and larger fractions of smaller organic acids.

The excitation–emission analysis of the methanol-soluble organic matter showed three distinct chromophores e.g., a less-oxygenated HULIS (LO-HULIS) component, a highly oxygenated HULIS (HO-HULIS) component, and a phenolic-like substance (PLS) component. Chromophores like PLS and LO-HULIS dominated the total fluorescence of primary organic aerosol with a relative fraction of 88 ± 7%. After photooxidaiton, the PLS chromophore significantly decreased from 46 ± 8% to 11 ± 6%. Assuming typical ambient OH concentrations (~1.5×10^6 molec cm^{-3}) and the laboratory photooxidation timescale (5.4×10^{11} molecules cm^{-3} s in experiment, equivalent to 4 days of atmospheric aging), the implied atmospheric lifetime of PLS is on the order of a few days. PLS can serve as a source-specific tracer only for very fresh combustion plumes. However, humic-like substances increased from 44%–55% observed for the primary samples to 77%–91% of the aged BrC, especially for the HO-HULIS chromophore. This points to photooxidation as a net formation pathway for HO-HULIS formation.

Links between PARAFAC components and molecuels detected by FIAERO-CIMS show that the HULIS chromophores are higher oxidation state and contained higher fractions of nitrogen containing molecules. In contrast, the PLS chromophore had a lower oxidation state and contained low fraction of nitrogen containing molecules. After photooxidation, the PLS chromophores fraction decreased. The oxidation of volatile organic compounds and degradation of large molecules generated smaller organic compounds with higher oxidation state and the high fractions of nitrogen containing molecules. However, this study has not yet achieved quantitative characterization of each individual process contributing to HULIS

chormophore formation. Future studies need to integrate isotopic techniques or mass spectromters to address this limitation and accurately quantify the contribution of each process. These mechanisms will help to understand evolution process of the chromophores from primary combustion emissions during the real atmospheric transportation and also provide information about not only the absorbance of light by the aerosols but also their emission spectra. Overall, this study provides insight into chromophore variations and chemical compositions of brown carbon aerosol from fresh burning combustion emissions and those after photooxidation using a FIGAERO-CIMS mass spectrometer and an excitation emission spectroscopy.

Data availability.

Data are available upon request to the corresponding author.

Author contributions

JZ, FJ, RM, ND, KL, and DB conducted the burning experiments. JZ helped to collect the filters. FJ analysed the filters by FIGAERO-CIMS and Aqualog in the laboratory, did the CIMS and Aqualog data analysis, produced all figures, and wrote the paper. CH and TL gave general comments. HS gave general advice and comments for this paper. All authors provided suggestions for the data analysis, interpretation, and discussion, and contributed to the final text.

Competing interests

The authors declare that there are no competing interests. Please note that some co-authors are co-editors of the journal.

ACKNOWLEDGMENTS

The authors gratefully thank the staff at PSI for providing substantial technical support during the burning experiment. We also would like to thank Pascal André Schneider from the Paul Scherrer Institute for building the holding tank and burning platform. Furthermore, Feng Jiang is thankful for the support from the China Scholarship Council (CSC) and AUST Foundation.

Financial support

Feng Jiang has received support from the Foundation of Anhui University of Science and Technology (award no. 2026yjc007).

510

REFERENCES

Bhattarai, H., Saikawa, E., Wan, X., Zhu, H. X., Ram, K., Gao, S. P., Kang, S. C., Zhang, Q. G., Zhang, Y. L., Wu, G. M., Wang, X. P., Kawamura, K., Fu, P. Q., and Cong, Z. Y.: Levoglucosan as a tracer of biomass burning: Recent progress and perspectives, Atmos. Res., 220, 20–33, https://doi.org/10.1016/j.atmosres.2019.01.004, 2019.

Bluvshtein, N., Lin, P., Flores, J. M., Segev, L., Mazar, Y., Tas, E., Snider, G., Weagle, C., Brown, S. S., Laskin, A., and Rudich, Y.: Broadband optical properties of biomass-burning aerosol and identification of brown carbon chromophores, J. Geophys. Res. Atmos., 122, 5441–5456, https://doi.org/10.1002/2016jd026230, 2017.

Bogler, S., Zhang, J., Cheung, R. K. Y., Li, K., Prévôt, A. S. H., El Haddad, I., and Bell, D. M.: Ozonolysis of primary biomass burning organic aerosol particles: insights into reactivity and phase state, Atmos. Chem. Phys., 25, https://doi.org/10229–10243, 10.5194/acp-25-10229-2025, 2025.

Cai, J., Wu, C., Wang, J., Du, W., Zheng, F., Hakala, S., Fan, X., Chu, B., Yao, L., Feng, Z., Liu, Y., Sun, Y., Zheng, J., Yan, C., Bianchi, F., Kulmala, M., Mohr, C., and Daellenbach, K. R.: Influence of organic aerosol molecular composition on particle absorptive properties in autumn Beijing, Atmos. Chem. Phys., 22, 1251–1269, https://doi.org/10.5194/acp-22-1251-2022, 2022.

Census of India: Households by Availability of Separate Kitchen and Type of Fuel Used for Cooking, available at: https: //censusindia.gov.in/census.website/data/census-tables (last access: 2 November 2023), 2011.

Chen, Q., Hua, X., and Dyussenova, A.: Evolution of the chromophore aerosols and its driving factors in summertime Xi'an, Northwest China, Chemosphere, 281, 130838, https://doi.org/10.1016/j.chemosphere.2021.130838, 2021a.

Chen, Q. C., Hua, X. Y., Li, J. W., Chang, T., and Wang, Y. Q.: Diurnal evolutions and sources of water-soluble chromophoric aerosols over Xi'an during haze event, in Northwest China, Sci. Total Environ., 786, https://doi.org/10.1016/j.scitotenv.2021.147412, 2021b.

Chen, Q. C., Li, J. W., Hua, X. Y., Jiang, X. T., Mu, Z., Wang, M. M., Wang, J., Shan, M., Yang, X. D., Fan, X. J., Song, J. Z., Wang, Y. Q., Guan, D. J., and Du, L.: Identification of species and sources of atmospheric chromophores by fluorescence excitation-emission matrix with parallel factor analysis, Sci. Total Environ., 718, https://doi.org/10.1016/j.scitotenv.2020.137322, 2020.

Chen, Q. C., Miyazaki, Y., Kawamura, K., Matsumoto, K., Coburn, S., Volkamer, R., Iwamoto, Y., Kagami, S., Deng, Y. G., Ogawa, S., Ramasamy, S., Kato, S., Ida, A., Kajii, Y., and Mochida, M.: Characterization of Chromophoric Water-Soluble Organic Matter in Urban, Forest, and Marine Aerosols by HR-ToF-AMS Analysis and Excitation Emission Matrix Spectroscopy, Environ. Sci. Technol., 50, 10351–10360, https://doi.org/10.1021/acs.est.6b01643, 2016.

Cory, R. M. and McKnight, D. M.: Fluorescence spectroscopy reveals ubiquitous presence of oxidized and reduced quinones in dissolved organic matter, Environ. Sci. Technol., 39, 8142–8149, https://doi.org/10.1021/es0506962, 2005.

Courtemanche, B. and Levendis, Y. A.: A laboratory study on the NO, NO2, SO2, CO and CO2 emissions from the combustion of pulverized coal, municipal waste plastics and tires, Fuel, 77, 183–196, https://doi.org/10.1016/S0016-2361(97)00191-9, 1998.

Deng, J., Ma, H., Wang, X., Zhong, S., Zhang, Z., Zhu, J., Fan, Y., Hu, W., Wu, L., Li, X., Ren, L., Pavuluri, C. M., Pan, X., Sun, Y., Wang, Z., Kawamura, K., and Fu, P.: Measurement report: Optical properties and sources of water-soluble brown carbon in Tianjin, North China – insights from organic molecular compositions, Atmos. Chem. Phys., 22, 6449–6470, https://doi.org/10.5194/acp-22-6449-2022, 2022.

Fan, X. J., Cao, T., Yu, X. F., Wang, Y., Xiao, X., Li, F. Y., Xie, Y., Ji, W. C., Song, J. Z., and Peng, P. A.: The evolutionary behavior of chromophoric brown carbon during ozone aging of fine particles from biomass burning, Atmos. Chem. Phys., 20, 4593–4605, https://doi.org/10.5194/acp-20-4593-2020, 2020.

Feng, Y., Ramanathan, V., and Kotamarthi, V. R.: Brown carbon: a significant atmospheric absorber of solar radiation?, Atmos. Chem. Phys., 13, 8607–8621, https://doi.org/10.5194/acp-13-8607-2013, 2013.

Fleming, L. T., Lin, P., Roberts, J. M., Selimovic, V., Yokelson, R., Laskin, J., Laskin, A., and Nizkorodov, S. A.: Molecular composition and photochemical lifetimes of brown carbon chromophores in biomass burning organic aerosol, Atmos. Chem. Phys., 20, 1105–1129, https://doi.org/10.5194/acp-20-1105-2020, 2020.

Haque, M. M., Kawamura, K., Deshmukh, D. K., Fang, C., Song, W., Mengying, B., and Zhang, Y. L.: Characterization of organic aerosols from a Chinese megacity during winter: predominance of fossil fuel combustion, Atmos. Chem. Phys., 19, 5147–5164, https://doi.org/10.5194/acp-19-5147-2019, 2019.

Huang, R. J., Yang, L., Shen, J. C., Yuan, W., Gong, Y. Q., Ni, H. Y., Duan, J., Yan, J., Huang, H. B., You, Q. H., and Li, Y. J.: Chromophoric Fingerprinting of Brown Carbon from Residential Biomass Burning, Environ. Sci. Technol. Lett., 9, 102–111, https://doi.org/10.1021/acs.estlett.1c00837, 2021.

Huang, W., Saathoff, H., Shen, X., Ramisetty, R., Leisner, T., and Mohr, C.: Chemical Characterization of Highly Functionalized Organonitrates Contributing to Night-Time Organic Aerosol Mass Loadings and Particle Growth, Environ. Sci. Technol., 53, 1165–1174, https://doi.org/10.1021/acs.est.8b05826, 2019.

Jiang, F., Saathoff, H., Ezenobi, U., Song, J., Zhang, H., Gao, L., and Leisner, T.: Measurement report: Brown carbon aerosol in rural Germany – sources, chemistry, and diurnal variations, Atmos. Chem. Phys., 25, 1917–1930, https://doi.org/10.5194/acp-25-1917-2025, 2025.

Jiang, F., Siemens, K., Linke, C., Li, Y., Gong, Y., Leisner, T., Laskin, A., and Saathoff, H.: Molecular analysis of secondary organic aerosol and brown carbon from the oxidation of indole, Atmos. Chem. Phys., 24, 2639–2649, https://doi.org/10.5194/acp-24-2639-2024, 2024.

Jiang, F., Song, J., Bauer, J., Gao, L., Vallon, M., Gebhardt, R., Leisner, T., Norra, S., and Saathoff, H.: Chromophores and chemical composition of brown carbon characterized at an urban kerbside by excitation–emission spectroscopy and mass spectrometry, Atmos. Chem. Phys., 22, 14971–14986, https://doi.org/10.5194/acp-22-14971-2022, 2022.

Kodros, J. K., Papanastasiou, D. K., Paglione, M., Masiol, M., Squizzato, S., Florou, K., Skyllakou, K., Kaltsonoudis, C., Nenes, A., and Pandis, S. N.: Rapid dark aging of biomass burning as an overlooked source of oxidized organic aerosol, Proc. Natl. Acad. Sci., 117, 33028–33033, https://doi.org/10.1073/pnas.2010365117, 2020.

Kodros, J. K., Kaltsonoudis, C., Paglione, M., Florou, K., Jorga, S., Vasilakopoulou, C., Cirtog, M., Cazaunau, M., Picquet-Varrault, B., Nenes, A., and Pandis, S. N.: Secondary aerosol formation during the dark oxidation of residential biomass burning emissions, Environ. Sci.: Atmos., 2, 1221–1236, https://doi.org/10.1039/D2EA00031H, 2022.

Kong, X. R., Salvador, C. M., Carlsson, S., Pathak, R., Davidsson, K. O., Le Breton, M., Gaita, S. M., Mitra, K., Hallquist, A. M., Hallquist, M., and Pettersson, J. B. C.: Molecular characterization and optical properties of primary emissions from a residential wood burning boiler, Sci. Total Environ., 754, https://doi.org/10.1016/j.scitotenv.2020.142143, 2021.

Laskin, A., Laskin, J., and Nizkorodov, S. A.: Chemistry of Atmospheric Brown Carbon, Chem. Rev., 115, 4335–4382, https://doi.org/10.1021/cr5006167, 2015.

Laskin, A., West, C. P., and Hettiyadura, A. P. S.: Molecular insights into the composition, sources, and aging of atmospheric brown carbon, Chem. Soc. Rev., https://doi.org/10.1039/D3CS00609C, 2025.

Li, C. L., He, Q. F., Fang, Z., Brown, S. S., Laskin, A., Cohen, S. R., and Rudich, Y.: Laboratory Insights into the Diel Cycle of Optical and Chemical Transformations of Biomass Burning Brown Carbon Aerosols, Environ. Sci. Technol., 54, 11827–11837, https://doi.org/10.1021/acs.est.0c04310, 2020.

Li, K., Zhang, J., Bell, D. M., Wang, T., Lamkaddam, H., Cui, T., Qi, L., Surdu, M., Wang, D., Du, L., El Haddad, I., Slowik, J. G., and Prevot, A. S. H.: Uncovering the dominant contribution of intermediate volatility compounds in secondary organic aerosol formation from biomass-burning emissions, Natl. Sci. Rev., 11, https://doi.org/10.1093/nsr/nwae014, 2024.

Lin, P., Aiona, P. K., Li, Y., Shiraiwa, M., Laskin, J., Nizkorodov, S. A., and Laskin, A.: Molecular Characterization of Brown Carbon in Biomass Burning Aerosol Particles, Environ. Sci. Technol., 50, 11815–11824, https://doi.org/10.1021/acs.est.6b03024, 2016.

Lin, P., Bluvshtein, N., Rudich, Y., Nizkorodov, S. A., Laskin, J., and Laskin, A.: Molecular Chemistry of Atmospheric Brown Carbon Inferred from a Nationwide Biomass Burning Event, Environ. Sci. Technol., 51, 11561–11570, https://doi.org/10.1021/acs.est.7b02276, 2017.

Lopez-Hilfiker, F. D., Mohr, C., Ehn, M., Rubach, F., Kleist, E., Wildt, J., Mentel, T. F., Lutz, A., Hallquist, M., Worsnop, D., and Thornton, J. A.: A novel method for online analysis of gas and particle composition: description and evaluation of a Filter Inlet for Gases and AEROsols (FIGAERO), Atmos. Meas. Tech., 7, 983–1001, https://doi.org/10.5194/amt-7-983-2014, 2014.

Mohr, C., Lopez-Hilfiker, F. D., Zotter, P., Prevot, A. S. H., Xu, L., Ng, N. L., Herndon, S. C., Williams, L. R., Franklin, J. P., Zahniser, M. S., Worsnop, D. R., Knighton, W. B., Aiken, A. C., Gorkowski, K. J., Dubey, M. K., Allan, J. D., and Thornton, J. A.: Contribution of Nitrated Phenols to Wood Burning Brown Carbon Light Absorption in Detling, United Kingdom during Winter Time, Environ. Sci. Technol., 47, 6316–6324, https://doi.org/10.1021/es400683v, 2013.

Moise, T., Flores, J. M., and Rudich, Y.: Optical Properties of Secondary Organic Aerosols and Their Changes by Chemical Processes, Chem. Rev., 115, 4400–4439, https://doi.org/10.1021/cr5005259, 2015.

Moschos, V., Kumar, N. K., Daellenbach, K. R., Baltensperger, U., Prevot, A. S. H., and El Haddad, I.: Source Apportionment of Brown Carbon Absorption by Coupling Ultraviolet-Visible Spectroscopy with Aerosol Mass Spectrometry, Environ. Sci. Technol. Lett., 5, 6, https://doi.org/10.1021/acs.estlett.8b00118, 2018.

Murphy, K. R., Stedmon, C. A., Graeber, D., and Bro, R.: Fluorescence spectroscopy and multi-way techniques. PARAFAC, Anal. Methods, 5, 6557–6566, https://doi.org/10.1039/c3ay41160e, 2013.

Pucher, M., Wunsch, U., Weigelhofer, G., Murphy, K., Hein, T., and Graeber, D.: staRdom: Versatile Software for Analyzing Spectroscopic Data of Dissolved Organic Matter in R, Water, 11, https://doi.org/10.3390/w11112366, 2019.

Saleh, R.: From Measurements to Models: Toward Accurate Representation of Brown Carbon in Climate Calculations, Curr. Pollut. Rep., 6, 90–104, https://doi.org/10.1007/s40726-020-00139-3, 2020.

Salvador, C. M. G., Tang, R. Z., Priestley, M., Li, L. J., Tsiligiannis, E., Le Breton, M., Zhu, W. F., Zeng, L. M., Wang, H., Yu, Y., Hu, M., Guo, S., and Hallquist, M.: Ambient nitro-aromatic compounds - biomass burning versus secondary formation in rural China, Atmos. Chem. Phys., 21, 1389–1406, https://doi.org/10.5194/acp-21-1389-2021, 2021.

Sardena, C., Gemmell, K. J., Zhang, J., Jiang, F., Saathoff, H., Bell, D. M., and Borduas-Dedekind, N.: Singlet Oxygen and Triplet Excited State Organics Produced by Primary Biomass Burning Organic Aerosol from Wood, Dung, Straw, and Plastic Fuels: Role of Solvent-Dependent Photochemistry, ACS ES&T Air, 3, 611–626, https://doi.org/10.1021/acsestair.5c00462, 2026.

Shrivastava, M., Cappa, C. D., Fan, J. W., Goldstein, A. H., Guenther, A. B., Jimenez, J. L., Kuang, C., Laskin, A., Martin, S. T., Ng, N. L., Petaja, T., Pierce, J. R., Rasch, P. J., Roldin, P., Seinfeld, J. H., Shilling, J., Smith, J. N., Thornton, J. A., Volkamer, R., Wang, J., Worsnop, D. R., Zaveri, R. A., Zelenyuk, A., and Zhang, Q.: Recent advances in understanding secondary organic aerosol: Implications for global climate forcing, Rev. Geophys., 55, 509–559, https://doi.org/10.1002/2016rg000540, 2017.

Simoneit, B. R. T.: Biomass burning — a review of organic tracers for smoke from incomplete combustion, Appl. Geochem., 17, 129–162, https://doi.org/10.1016/S0883-2927(01)00061-0, 2002.

Smith, K. R., Bruce, N., Balakrishnan, K., Adair-Rohani, H., Balmes, J., Chafe, Z., Dherani, M., Hosgood, H. D., Mehta, S., Pope, D., and Rehfuess, E.: Millions Dead: How Do We Know and What Does It Mean?

Methods Used in the Comparative Risk Assessment of Household Air Pollution, Annu. Rev. Public Health, 35, 185–206, https://doi.org/10.1146/annurevpublhealth-032013-182356, 2014.

Song, J., Li, M., Zou, C., Cao, T., Fan, X., Jiang, B., Yu, Z., Jia, W., and Peng, P. a.: Molecular Characterization of Nitrogen-Containing Compounds in Humic-like Substances Emitted from Biomass Burning and Coal Combustion, Environ. Sci. Technol., 56, 119–130, https://doi.org/10.1021/acs.est.1c04451, 2022.

Stubbins, A., Lapierre, J. F., Berggren, M., Prairie, Y. T., Dittmar, T., and del Giorgio, P. A.: What's in an EEM? Molecular Signatures Associated with Dissolved Organic Fluorescence in Boreal Canada, Environ. Sci. Technol., 48, 10598–10606, https://doi.org/10.1021/es502086e, 2014.

Sumlin, B. J., Pandey, A., Walker, M. J., Pattison, R. S., Williams, B. J., and Chakrabarty, R. K.: Atmospheric Photooxidation Diminishes Light Absorption by Primary Brown Carbon Aerosol from Biomass Burning, Environ. Sci. Technol. Lett., 4, 540–545, https://doi.org/10.1021/acs.estlett.7b00393, 2017.

Tang, J., Li, J., Su, T., Han, Y., Mo, Y. Z., Jiang, H. X., Cui, M., Jiang, B., Chen, Y. J., Tang, J. H., Song, J. Z., Peng, P. A., and Zhang, G.: Molecular compositions and optical properties of dissolved brown carbon in biomass burning, coal combustion, and vehicle emission aerosols illuminated by excitation-emission matrix spectroscopy and Fourier transform ion cyclotron resonance mass spectrometry analysis, Atmos. Chem. Phys., 20, 2513–2532, https://doi.org/10.5194/acp-20-2513-2020, 2020.

Tang, J., Li, J., Zhao, S., Zhong, G., Mo, Y., Jiang, H., Jiang, B., Chen, Y., Tang, J., Tian, C., Zong, Z., Hussain Syed, J., Song, J., and Zhang, G.: Molecular signatures and formation mechanisms of water-soluble chromophores in particulate matter from Karachi in Pakistan, Sci. Total Environ., 914, 169890, https://doi.org/10.1016/j.scitotenv.2024.169890, 2024.

Wang, T. T., Zhang, J., Lamkaddam, H., Li, K., Cheung, K. Y., Kattner, L., Gammelsaeter, E., Bauer, M., Decker, Z. C. J., Bhattu, D., Huang, R. J., Modini, R. L., Slowik, J. G., El Haddad, I., Prevot, A. S. H., and Bell, D. M.: Chemical characterization of organic vapors from wood, straw, cow dung, and coal burning, Atmos. Chem. Phys., 25, 2707–2724, https://doi.org/10.5194/acp-25-2707-2025, 2025.

Washenfelder, R. A., Attwood, A. R., Brock, C. A., Guo, H., Xu, L., Weber, R. J., Ng, N. L., Allen, H. M., Ayres, B. R., Baumann, K., Cohen, R. C., Draper, D. C., Duffey, K. C., Edgerton, E., Fry, J. L., Hu, W. W., Jimenez, J. L., Palm, B. B., Romer, P., Stone, E. A., Wooldridge, P. J., and Brown, S. S.: Biomass

burning dominates brown carbon absorption in the rural southeastern United States, Geophys. Res. Lett., 42, 653–664, https://doi.org/10.1002/2014GL062444, 2015.

Winter, F., Wartha, C., and Hofbauer, H.: NO and N2O formation during the combustion of wood, straw, malt waste and peat, Bioresour. Technol., 70, 39–49, https://doi.org/10.1016/S0960-8524(99)00019-X, 1999.

Wu, G., Wan, X., Gao, S., Fu, P., Yin, Y., Li, G., Zhang, G., Kang, S., Ram, K., and Cong, Z.: Humic-like substances (HULIS) in aerosols of central Tibetan Plateau (Nam Co, 4730 m asl): Abundance, light absorption properties and sources, Environ. Sci. Technol., 52, 7203-7211, https://doi.org/10.1021/acs.est.8b01251, 2018.

Xie, M., Chen, X., Hays, M. D., Lewandowski, M., Offenberg, J., Kleindienst, T. E., and Holder, A. L.: Light Absorption of Secondary Organic Aerosol: Composition and Contribution of Nitroaromatic Compounds, Environ. Sci. Technol., 51, 11607–11616, https://doi.org/10.1021/acs.est.7b03263, 2017.

Xiong, R., Li, J., Zhang, Y., Zhang, L., Jiang, K., Zheng, H., Kong, S., Shen, H., Cheng, H., Shen, G., and Tao, S.: Global brown carbon emissions from combustion sources, Environ. Sci. Ecotechnology., 12, 100201, https://doi.org/10.1016/j.ese.2022.100201, 2022.

Yan, G. and Kim, G.: Speciation and Sources of Brown Carbon in Precipitation at Seoul, Korea: Insights from Excitation-Emission Matrix Spectroscopy and Carbon Isotopic Analysis, Environ. Sci. Technol., 51, 11580–11587, https://doi.org/10.1021/acs.est.7b02892, 2017.

Yang, Z., Tsona, N. T., George, C., and Du, L.: Nitrogen-Containing Compounds Enhance Light Absorption of Aromatic-Derived Brown Carbon, Environ. Sci. Technol., 10.1021/acs.est.1c08794, 2022.

Yazdani, A., Takahama, S., Kodros, J. K., Paglione, M., Masiol, M., Squizzato, S., Florou, K., Kaltsonoudis, C., Jorga, S. D., Pandis, S. N., and Nenes, A.: Chemical evolution of primary and secondary biomass burning aerosols during daytime and nighttime, Atmos. Chem. Phys., 23, 7461–7477, https://doi.org/10.5194/acp-23-7461-2023, 2023.

Yue, S., Zhu, J., Chen, S., Xie, Q., Li, W., Li, L., Ren, H., Su, S., Li, P., Ma, H., Fan, Y., Cheng, B., Wu, L., Deng, J., Hu, W., Ren, L., Wei, L., Zhao, W., Tian, Y., Pan, X., Sun, Y., Wang, Z., Wu, F., Liu, C.-Q., Su, H., Penner, J. E., Pöschl, U., Andreae, M. O., Cheng, Y., and Fu, P.: Brown carbon from biomass burning imposes strong circum-Arctic warming, One Earth, 5, 293–304, https://doi.org/10.1016/j.oneear.2022.02.006, 2022.

Zeng, L. H., Zhang, A. X., Wang, Y. H., Wagner, N. L., Katich, J. M., Schwarz, J. P., Schill, G. P., Brock, C., Froyd, K. D., Murphy, D. M., Williamson, C. J., Kupc, A., Scheuer, E., Dibb, J., and Weber, R. J.: Global Measurements of Brown Carbon and Estimated Direct Radiative Effects, Geophys. Res. Lett., 47, https://doi.org/10.1029/2020gl088747, 2020.

Zhang, J., Li, K., Wang, T., Gammelsæter, E., Cheung, R. K. Y., Surdu, M., Bogler, S., Bhattu, D., Wang, D. S., Cui, T., Qi, L., Lamkaddam, H., El Haddad, I., Slowik, J. G., Prevot, A. S. H., and Bell, D. M.: Bulk and molecular-level composition of primary organic aerosol from wood, straw, cow dung, and plastic burning, Atmos. Chem. Phys., 23, 14561–14576, https://doi.org/10.5194/acp-23-14561-2023, 2023.

Zhang, L., Hu, B., Liu, X., Luo, Z., Xing, R., Li, Y., Xiong, R., Li, G., Cheng, H., Lu, Q., Shen, G., and Tao, S.: Variabilities in Primary N-Containing Aromatic Compound Emissions from Residential Solid Fuel Combustion and Implications for Source Tracers, Environ. Sci. Technol., 56, 13622–13633, https://doi.org/10.1021/acs.est.2c03000, 2022.

Zhu, C.-S., Qu, Y., Huang, H., Shi, J.-L., Dai, W.-T., Zhang, N.-N., Wang, N., Wang, L.-Y., Ji, S.-S., and Cao, J.-J.: Brown Carbon From Biomass Burning Reinforces the Himalayas and Tibetan Plateau Warming, Geophys. Res. Lett., 51, e2023GL107269, https://doi.org/10.1029/2023GL107269, 2024.